Stacking-dependent topological quantum states in bilayer $Mn_2Cl_3Br_3$

Xinlei Zhao,[1,2] Peng-Jie Guo,[3] Fengjie Ma,[1,2,*] and Zhong-Yi Lu[3]

[1]*The Center for Advanced Quantum Studies and Department of Physics, Beijing Normal University, Beijing 100875, China*
[2]*Key Laboratory of Multiscale Spin Physics (Ministry of Education), Beijing Normal University, Beijing 100875, China*
[3]*Department of Physics, Renmin University of China, Beijing 100872, China*

(Received 17 November 2022; accepted 16 June 2023; published 21 July 2023)

Stacking-dependent physics is emerging as a fascinating research topic for two-dimensional materials. A variety of novel properties can be achieved by layer stacking according to different modes. However, most of the studies focus on the impact of electronic, superconducting, optical, and magnetic properties. In this work, we have systematically studied the stacking-dependent topological quantum states in bilayer $Mn_2Cl_3Br_3$ by the first-principles electronic structure calculations. Here, ferromagnetic layer coupling is always favored in different stacking modes. Many exotic topological quantum states, such as topological nodal-ring spin-gapless semimetal state, spin-valley polarized quantum valley Hall (SVP-QVH) effect, and high Chern number quantum anomalous Hall effect can be realized in this single system. Among these states, the SVP-QVH is a new topological phase discovered for the first time, in which there are two topologically protected gapless chiral edge states that carry the same spin, localize respectively on the two polarized valleys, and propagate in opposite directions along the edges. The spin-valley polarized anomalous valley Hall effect can be further realized with electron doping or gate tuning, resulting in edge states that integrate multiple degrees of freedom of valley, spin, and charge. Our research therefore provides an idea for discovery of new topological phases and design of two-dimensional multifunctional electronic, spintronic, and topological devices.

DOI: 10.1103/PhysRevResearch.5.033040

I. INTRODUCTION

Due to the reduced dimensionality and symmetry, two-dimensional (2D) materials exhibit lots of fantastic and unique characteristics in electronic, magnetic, thermal, and mechanical properties, and thus have attracted tremendous interest from researchers in varying fields [1–4]. In recent years, the stacking-dependent phenomena in 2D bilayer structures are emerging as a fascinating topic, disclosing novel physical properties that are critical for state-of-the-art technological applications [5–21].

In bilayer materials, two 2D atomically thin layers stack vertically together by van der Waals interactions, giving rise to not only the possibility of combining the inherent properties of each layer, but also the possibility of emerging properties far beyond those of the individuals [4–13]. The extra layer degree of freedom in bilayer materials can result in rich phase diagram [4–9]. Moreover, since the interlayer coupling can be adjusted flexibly by interacting with different surfaces, resulting in stacking-dependent electronic properties, the physical properties of bilayer system can be precisely engineered. The most well-known example of stacking-dependent 2D system is bilayer graphene, in which two graphene monolayers are stacked together with small twisted angles, resulting in the vanishing of Fermi velocity and the development of flat energy bands hosting domes of superconductivity, thus opening the era of twistronics [14,15]. Another typical example is bilayer CrI_3, whose magnetic ground state can be modulated by changing the stacking configurations [19]. However, despite the increased efforts devoted to the field, studies of stacking-dependent phenomena in 2D systems have so far mainly focused on the electronic, superconducting, optical, and magnetic properties [16–19]. There is only very limited exploration of whether stacking-dependent phenomena can be extended to topological properties [21], which would be of fundamental interest and greatly enrich the stacking-dependent physics of bilayer structures.

Recently, the experimentally synthesized 2D Janus monolayers become an exciting new class of materials that exhibit unique optical, electronic, valleytronic, and topological properties [22–29], such as Janus graphene with powerful surfactants [22], Janus transition metal dichalcogenide MoSSe that shows high basal plane hydrogen evolution reaction activity, topological, and ferroelastic properties [23–25]. In comparison with their prototypes MX_2 (M and X represent transition metal and chalcogen element, respectively), 2D Janus materials have an asymmetric out-of-plane structural configurations of different elements on the upper and lower surfaces, which breaks the space-inversion symmetry or mirror-z (M_z) symmetry, and thus can induce many superior properties [26–29].

As we have known, if the space-inversion and time-reversal symmetries simultaneously exist in a system, Berry

*fengjie.ma@bnu.edu.cn

Published by the American Physical Society under the terms of the Creative Commons Attribution 4.0 International license. Further distribution of this work must maintain attribution to the author(s) and the published article's title, journal citation, and DOI.

curvature will vanish in the entire Brillouin zone (BZ) [30]. For 2D Janus materials with hexagonal lattices, the breaking of space-inversion symmetry not only results in nonzero Berry curvature, but also lifts the degeneracy of K and K′ valleys, leading to a controllable valley pseudospin degree of freedom [31]. The valleys possess opposite spin splittings, Berry curvatures, and orbital magnetic moments, which can generate exotic physics, such as the valley Hall effect and optical circular dichroism [28,29,32]. If the materials have intrinsic magnetism that further breaks the time-reversal symmetry, they can host the quantum anomalous Hall (QAH) effect and topologically protected chiral edge states which carry dissipationless current, providing a fertile platform for realizing low energy consumption and dissipationless spintronic devices [33–44]. The combination of topological and valley physical properties therefore makes 2D Janus materials a promising candidate for future technological applications. However, despite intensive research for decades, the reports of 2D Janus materials with intrinsic magnetism are still very rare. Recently, several magnetic 2D Janus monolayers have been theoretically proposed [45–49], exhibiting many exotic physical properties, such as the QAH effect [46], valley polarization [48], and enhanced Curie temperature [49].

In this work, based on the first-principles electronic structure calculations, we have systematically studied the stacking-dependent electronic and topological properties of bilayer $Mn_2Cl_3Br_3$, whose monolayer is an intrinsic ferromagnetic QAH system. Many exotic topological quantum states beyond those of the monolayer, such as topological nodal-ring spin-gapless semimetal state, spin-valley polarized quantum valley Hall (SVP-QVH) effect, and high Chern number QAH (HC-QAH) effect, can be realized in this single system with different stacking modes. Our work reveals that these rich stacking-dependent, design-programmable properties of 2D Janus magnetic materials will greatly broaden the impact of bilayer materials in fundamental scientific research and technological applications.

II. COMPUTATIONAL DETAILS

In our calculations, the plane-wave basis based method and Quantum-ESPRESSO software package were used [50,51]. We adopted the generalized gradient approximation (GGA) of the Perdew-Burke-Ernzerhof formula for the exchange-correlation potentials [52]. The ultrasoft pseudopotentials were employed to model the electron-ion interactions [53]. A corrective Hubbard-like U term was introduced to treat the strong on-site Coulomb interaction of the localized electrons of the transition metal ions [54,55]. The effective values of U used in calculations was 4.0 eV for Mn-3d electrons. A mesh of $16 \times 16 \times 1$ k-points grid was used for sampling the BZ, and the Marzari-Vanderbilt broadening technique was adopted [56]. In order to avoid the residual interaction between adjacent layers, a 20 Å vacuum layer was used. After convergence tests, the kinetic energy cutoffs for wave functions and charge densities were chosen to be 60 and 480 Ry, respectively. During the simulations, all structural geometries were fully optimized to achieve the minimum energy. The edge states were studied using tight-binding methods by the combination of Wannier90 and WannierTools software packages [57,58].

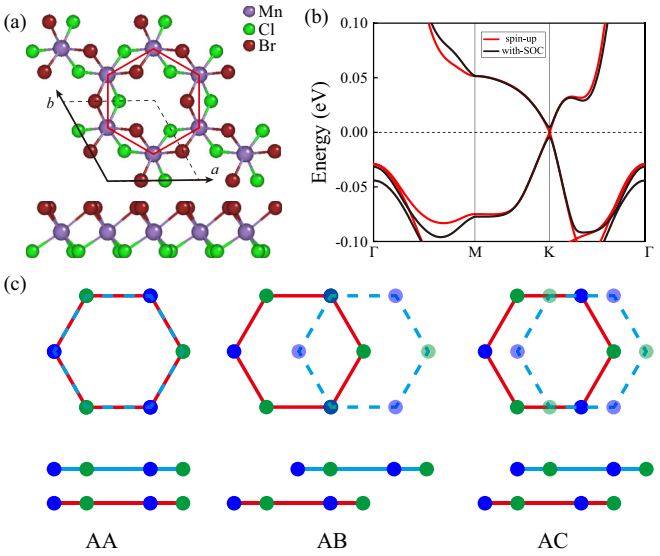

FIG. 1. (a) Top and side view of monolayer $Mn_2Cl_3Br_3$, in which the Mn, Cl, and Br atoms are located in three atomic layers denoted respectively by different colors. The black dashed line represents the unit cell, while the red solid hexagon shows the Mn lattice. (b) Band structure of monolayer $Mn_2Cl_3Br_3$ with/without SOC in the ferromagnetic ground state. In the absence of SOC, the minority spin has about a 4.1 eV energy gap at the Fermi level, and hence it is not visible in the energy window illustrated. (c) The top and side views of AA, AB, and AC stacking modes of bilayer $Mn_2Cl_3Br_3$. The red solid and cyan dashed lines represent the Mn lattice as illustrated in (a), and the blue and green spheres represent the two subsets of Mn atoms.

III. RESULTS AND DISCUSSION

A. Monolayer $Mn_2Cl_3Br_3$

The 2D Janus $Mn_2Cl_3Br_3$ monolayer crystallizes in a hexagonal structure with $P31m$ (No. 157) space group, as shown in Fig. 1(a), using the Device Studio program for visualization and modeling [59]. The 3d-metal Mn cations form a honeycomb lattice and are sandwiched between layers of two different halogen atoms Cl and Br. Due to the asymmetry of Janus structure, space-inversion symmetry is broken in $Mn_2Cl_3Br_3$ monolayer, resulting in a C_{3v} symmetry. In our calculations, a ferromagnetic ground state with an out-of-plane magnetic moment $\sim 4.0\,\mu_B$ per Mn atom is found, consistent with the previous report [46]. The material is dynamically stable [46], whose lattice constant is about 6.51 Å.

Figure 1(b) shows the calculated electronic band structures of monolayer $Mn_2Cl_3Br_3$ in the ferromagnetic ground state. In the absence of spin-orbit coupling (SOC), the 2D Janus $Mn_2Cl_3Br_3$ is a perfect half-semi-metal, whose majority spin exhibits a linearly crossing band dispersion and vanishing density of states at the Fermi level while the minority one has a large, ~4.1 eV, insulating band gap (not shown in the plotted energy window). A full (100%) spin polarization near the Fermi level is expected in $Mn_2Cl_3Br_3$ monolayer. The

states near the Fermi level are mainly contributed by Cl-3p and Br-4p orbitals. Once SOC is included in calculations, a ∼9 meV nontrivial energy gap is opened at the linear crossing point, accompanied by the emergence of a chiral edge state that is predicted to give rise to a QAH effect with Chern number $C = 1$ [46].

B. Bilayer $Mn_2Cl_3Br_3$

If we assemble two $Mn_2Cl_3Br_3$ monolayers vertically into a bilayer structure, different stacking patterns will endow the system with different symmetries, resulting in a variety of topological states, especially offering the possibility of emergent properties far beyond those of the monolayer. Figure 1(c) illustrates three stacking modes of bilayer $Mn_2Cl_3Br_3$, namely as AA, AB, and AC structures. The hexagonal lattice corresponds to the Mn lattice [the red hexagon shown in Fig. 1(a)], while the blue and green spheres represent the two subsets of Mn atoms in each layer. Our calculations reveal that ferromagnetic interlayer coupling is the most favorable interaction for the various stacking modes. If we set the energies of the states with ferromagnetic interlayer coupling to be zero as a reference, the relative energies of the states with antiferromagnetic interlayer coupling are about 0.1, 2.0, and 0.6 meV per unit cell for Cl-Cl neighbor; 5.9, 4.1, and 2.4 meV per unit cell for Br-Br neighbor; and 0.1, 0.6, and 0.4 meV per unit cell for Cl-Br neighbor with AA, AB, and AC stacking modes, respectively. This means that the ferromagnetic state is always the ground state for different stacking bilayer $Mn_2Cl_3Br_3$. In the following, we discuss in detail the topological quantum phases originating from the different stacking modes.

1. Nodal-ring semimetal state

If $Mn_2Cl_3Br_3$ monolayers are stacked with X-X (X = Cl or Br) AA mode, the bilayer system belongs to P-62 m (No. 189) space group with one M_z symmetry and three mirror symmetries perpendicular to the atomic layers. From our calculations, we find that different X-X (X = Cl or Br) AA patterns of bilayer $Mn_2Cl_3Br_3$ share similar electronic and topological properties. Here we take the Cl-Cl AA stacking pattern as a concrete example.

Without considering SOC, the internal spin space is decoupled from the real space. As shown in Fig. 2(a), there is only majority spin (spin up) near the Fermi level, while the minority one is insulating with a trivial band gap of ∼4.1 eV, indicating a 100% spin polarization. The conduction and valence bands of the majority spin intersect with each other at the Fermi level, forming two Weyl rings protected by the M_z symmetry. Once SOC is taken into account, the spin space couples with the real space, breaking the spin-rotation symmetry. Since the magnetic moments of Mn atoms are along the out-of-plane direction, the three vertical mirror symmetries parallel to the spin direction are destroyed, while the horizontal M_z symmetry perpendicular to the spin direction is preserved, resulting in the electronic band structure shown in Fig. 2(b). Since the highest valence and lowest conduction bands belong to two different irreducible representations, Γ_3 and Γ_4 of C_s double point group, their crossings (the Weyl points) at the Fermi level still exist, as they are protected by the M_z symmetry. Figure 2(c) shows the energy dispersions

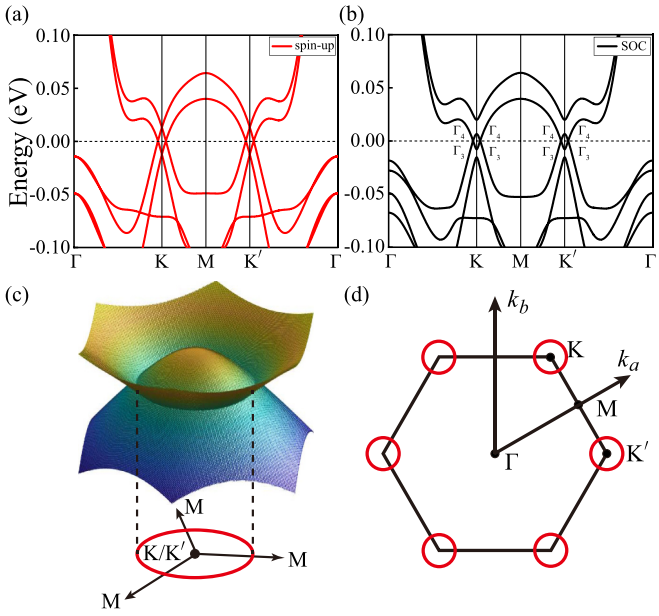

FIG. 2. Band structure of Cl-Cl AA stacking $Mn_2Cl_3Br_3$ (a) without and (b) with SOC in the ferromagnetic ground state. (c) The three dimensional energy dispersions of the highest valence and lowest conduction bands around K or K′ near the Fermi level. (d) The distribution of nodal-ring Weyl states in the BZ.

of the highest valence and lowest conduction bands around K or K′. The two bands intersect with each other, forming the flat nodalrings of Weyl points centered around K and K′, as shown in Fig. 2(d). The system is therefore manifested as a 2D spin-gapless topological nodal-ring semimetal. Moreover, this type of nodalring is characterized by fully spin polarized states near the Fermi level, which can avoid the spin current hybridization [60,61], different from the system with opposite spin-polarized states that coexist at the Fermi level [62,63].

2. SVP-QVH effect

The X-Y (Cl-Br or Br-Cl) AB stacking bilayer $Mn_2Cl_3Br_3$ belong to P3 (No. 143) space group, which has C_3 rotation symmetry along the z axis. The space-inversion symmetry and mirror symmetries are broken, which makes the two valleys K and K′ no longer equal to each other. In these stacking modes we choose Cl-Br AB stacking pattern as a concrete example.

Figure 3(a) shows the electronic band structure of Cl-Br AB stacking bilayer $Mn_2Cl_3Br_3$ in the absence of SOC. The system is a ferromagnetic semiconductor. A small energy gap, ∼5 meV, is opened for the majority spin, while the minority one is insulating with a trivial band gap of ∼4.1 eV. Once SOC is included in calculations, the valleys K and K′ become significantly different, as shown in Fig. 3(b). The band gaps around K and K′ points are ∼7 and ∼3 meV, respectively.

To further study the topological properties of the system, we calculate the Berry curvature, which arises as a consequence of either space-inversion symmetry breaking or time-reversal symmetry breaking in a system and is a

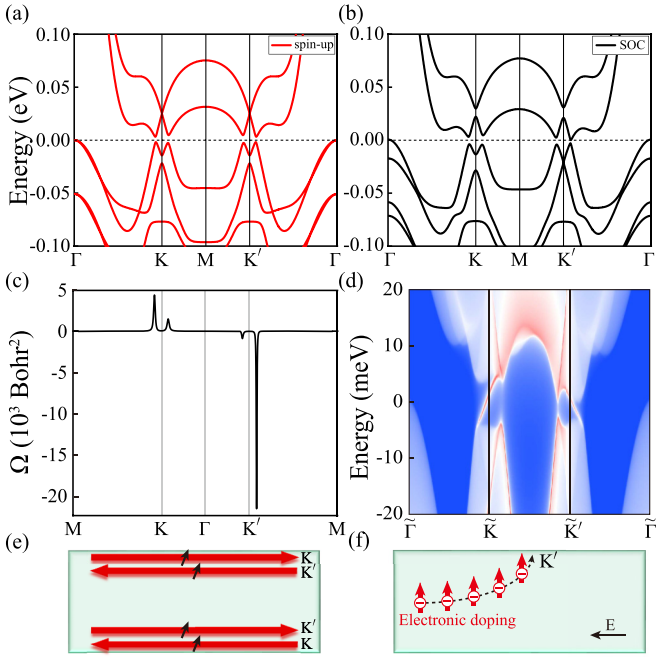

FIG. 3. (a) Band structure of Cl-Br AB stacking bilayer $Mn_2Cl_3Br_3$ (a) without and (b) with SOC in the ferromagnetic ground state. (c) The calculated Berry curvatures. (d) The edge states on the zigzag (100) edge. (e) Schematic showing the propagation direction of the edge states (the direction of an edge current, denoted by arrows) in the SVP-QVH phase. (f) Deflection of the carrier under in-plane longitudinal electric field.

paramount physical property that leads to interesting phenomena such as the valley Hall effect [64]. The Berry curvature for the nth band is defined as

$$\Omega_{nk} = -2\,\mathrm{Im}\sum_{n'\neq n}\frac{\langle n\boldsymbol{k}|v_x|n'\boldsymbol{k}\rangle\langle n'\boldsymbol{k}|v_y|n\boldsymbol{k}\rangle}{(\omega_{n'}-\omega_n)^2}, \tag{1}$$

in which v_x and v_y are the velocity operators. For 2D Bloch electrons, the total Chern number C_{tot} can be determined by the integration of the Berry curvature over the whole BZ:

$$C_{\mathrm{tot}} = \frac{1}{2\pi}\sum_n\int_{BZ} d^2\boldsymbol{k}\Omega_{nk}, \tag{2}$$

while the local Chern numbers at the K and K′ points, C_K and $C_{K'}$, are defined in half of the first BZ around K or K′, respectively [65]. The corresponding valley Chern number $C_v = C_K - C_{K'}$ is normally used to characterize the quantum valley Hall (QVH) effect.

As shown in Fig. 3(c), the Berry curvatures of Cl-Br AB stacking bilayer $Mn_2Cl_3Br_3$ show peaks with opposite signs around the two valleys, K and K′, generating a valley-dependent anomalous velocity at the boundary and opposite valley Chern numbers ($C_K = -C_{K'} = 1$). The calculated total Chern number is then $C_{\mathrm{tot}} = 0$ by integrating the Berry curvatures over the whole BZ, while the valley Chern number is $C_v = 2$, indicating a quantum valley Hall (QVH) effect in the system. Furthermore, within the bulk gap, there exist two fully spin-polarized topologically protected gapless chiral edge states localized on different valleys and propagated in opposite directions along the edges, as shown in Fig. 3(d). A feature in this system is that the pair of counter-propagating edge states in different valleys carry the same spin and originate from K and K′ valleys separately. Therefore, a spin-valley polarized quantum valley Hall (SVP-QVH) effect exists in the material. This is a phase that belongs to a type of QVH state but with both spin and valley polarized.

In Fig. 3(e), we schematically plot the spatial distribution and spin polarization of edge states for this new phase. Since the two states come from different valleys, they do not mix with each other on the edges. Compared with the QVH system, the valley properties of materials with SVP-QVH effect rely on the break of space-inversion symmetry. With electron doping or gate tuning, a net current with spin polarization can be generated on the K′ valley. When an in-plane longitudinal electric field is applied, the carrier will be deflected in transverse direction without an external magnetic field, generating anomalous valley Hall effect. Since the band structure is fully spin polarized around the Fermi level, the resulting net transverse Hall current is contributed by single spin, giving rise to spin-valley polarized anomalous valley Hall effect [31,66], as shown in Fig. 3(f). The combination of valleytronics and topological properties in Cl-Br AB-stacking bilayer $Mn_2Cl_3Br_3$ can yield many interesting applications, such as the valley controlled dissipationless spintronics.

3. HC-QAH effect

In this subsection, we reveal the HC-QAH effect of X-X (X = Cl or Br) and X-Y (Cl-Br or Br-Cl) AC stacking bilayer $Mn_2Cl_3Br_3$. The system belongs to the Cm (No. 8) space group, which has only one combined symmetry of time-reversal symmetry and mirror symmetry perpendicular to the atomic layers. Here, we take Br-Br AC stacking pattern as an example, since different X-X (X = Cl or Br) AC patterns of bilayer $Mn_2Cl_3Br_3$ share similar electronic and topological properties.

In the absence of SOC, the valence band and conduction band of Br-Br AC stacking bilayer $Mn_2Cl_3Br_3$, as well as the Fermi level, intersect linearly at the points near K and K′, which are protected by the vertical mirror symmetry, as shown in Fig. 4(a). The vertical mirror symmetry is broken once SOC is included, and hence a local gap is opened at the linear crossing points, as shown in Fig. 4(b).

The Berry curvatures of Br-Br AC stacking bilayer $Mn_2Cl_3Br_3$ show two sharp peaks around the valleys K and K′, as illustrated in Fig. 4(c). By integrating the Berry curvatures at the first BZ, a high Chern number of two is obtained. Figure 4(d) shows the edge states along the zigzag (100) direction, in which there are two topologically protected gapless chiral edge sates connecting the bulk valence and conduction bands in the valley K′. The two chiral edge states on the same boundary are located on the same valley and propagated in the same direction, whose number equals to the Chern number of two. Therefore, the system exhibits a high Chern number QAH phase with $C = 2$, which can provide an enhanced anomalous Hall conductivity due to the presence of two chiral edge states within the bulk gap leading to two QAH subsystems superimposed together.

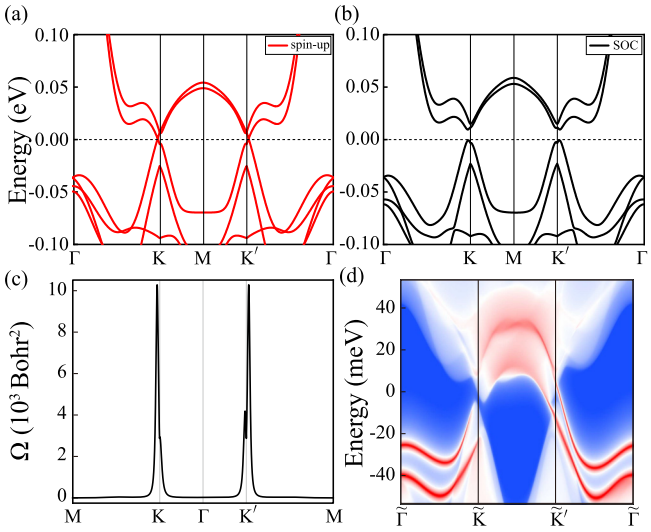

FIG. 4. (a) Band structure of Br-Br AC stacking bilayer $Mn_2Cl_3Br_3$ (a) without and (b) with SOC in the ferromagnetic ground state. (c) The calculated Berry curvatures. (d) The edge states on the zigzag (100) edge.

IV. CONCLUSION

In summary, by assembling 2D Janus $Mn_2Cl_3Br_3$ monolayers into a bilayer system, we can achieve various topological phases with different stacking modes, including a topological nodal-ring spin-gapless semimetal state, SVP-QVH state, and HC-QAH state, in which SVP-QVH is a new topological phase discovered in this work. In addition to the edge states counterpropagated in different valleys, the system with SVP-QVH is also characterized by spin polarization and valley polarization, upon which the spin-valley polarized anomalous valley Hall effect can be further realized by electron doping or gate tuning. Our findings therefore provide an excellent design-programmable platform and construction method for the future applications of topological physics combined with spintronics and valleytronics.

ACKNOWLEDGMENTS

This work was supported by the National Natural Science Foundation of China under Grants No. 12074040 and No. 12204533. The computations were supported by the Center for Advanced Quantum Studies, Beijing Normal University, and Hongzhiwei Technology.

[1] A. H. Castro Neto, F. Guinea, N. M. R. Peres, K. S. Novoselov, and A. K. Geim, The electronic properties of graphene, Rev. Mod. Phys. **81**, 109 (2009).

[2] S. Manzeli, D. Ovchinnikov, D. Pasquier, O. V. Yazyev, and A. Kis, 2D transition metal dichalcogenides, Nat. Rev. Mater. **2**, 17033 (2017).

[3] S. Z. Butler, S. M. Hollen, L. Cao, Y. Cui, J. A. Gupta, H. R. Gutiérrez, T. F. Heinz, S. S. Hong, J. Huang, A. F. Ismach, E. Johnston-Halperin, M. Kuno, V. V. Plashnitsa, R. D. Robinson, R. S. Ruoff, S. Salahuddin, J. Shan, L. Shi, M. G. Spencer, M. Terrones *et al.*, Progress, challenges, and opportunities in two-dimensional materials beyond graphene, ACS Nano **7**, 2898 (2013).

[4] K. S. Novoselov, A. Mishchenko, A. Carvalho, and A. H. Castro Neto, 2D materials and van der waals heterostructures, Science **353**, aac9439 (2016).

[5] A. K. Geim and I. V. Grigorieva, Van der waals heterostructures, Nature (London) **499**, 419 (2013).

[6] M.-C. Wang, C.-C. Huang, C.-H. Cheung, C.-Y. Chen, S. G. Tan, T.-W. Huang, Y. Zhao, Y. Zhao, G. Wu, Y.-P. Feng, H.-C. Wu, and C.-R. Chang, Prospects and opportunities of 2D van der waals magnetic systems, Ann. Phys. **532**, 1900452 (2020).

[7] C. Gong and X. Zhang, Two-dimensional magnetic crystals and emergent heterostructure devices, Science **363**, eaav4450 (2019).

[8] D. Jariwala, T. J. Marks, and M. C. Hersam, Mixed-dimensional van der waals heterostructures, Nat. Mater. **16**, 170 (2017).

[9] U. Chandni, K. Watanabe, T. Taniguchi, and J. P. Eisenstein, Signatures of phonon and defect-assisted tunneling in planar metal–hexagonal boron nitride–graphene junctions, Nano Lett. **16**, 7982 (2016).

[10] Z. Zhang, Y. Wang, K. Watanabe, T. Taniguchi, K. Ueno, E. Tutuc, and B. J. LeRoy, Flat bands in twisted bilayer transition metal dichalcogenides, Nat. Phys. **16**, 1093 (2020).

[11] Y. Zhang, T.-T. Tang, C. Girit, Z. Hao, M. C. Martin, A. Zettl, M. F. Crommie, Y. R. Shen, and F. Wang, Direct observation of a widely tunable bandgap in bilayer graphene, Nature (London) **459**, 820 (2009).

[12] I. K. Drozdov, A. Alexandradinata, S. Jeon, S. Nadj-Perge, H. Ji, R. J. Cava, B. Andrei Bernevig, and A. Yazdani, One-dimensional topological edge states of bismuth bilayers, Nat. Phys. **10**, 664 (2014).

[13] C. Zhang, C.-P. Chuu, X. Ren, M.-Y. Li, L.-J. Li, C. Jin, M.-Y. Chou, and C.-K. Shih, Interlayer couplings, moiré patterns, and 2D electronic superlattices in MoS_2/WSe_2 hetero-bilayers, Sci. Adv. **3**, e1601459 (2017).

[14] Y. Cao, V. Fatemi, S. Fang, K. Watanabe, T. Taniguchi, E. Kaxiras, and P. Jarillo-Herrero, Unconventional superconductivity in magic-angle graphene superlattices, Nature (London) **556**, 43 (2018).

[15] Y. Cao, V. Fatemi, A. Demir, S. Fang, S. L. Tomarken, J. Y. Luo, J. D. Sanchez-Yamagishi, K. Watanabe, T. Taniguchi, E. Kaxiras, R. C. Ashoori, and P. Jarillo-Herrero, Correlated insulator behaviour at half-filling in magic-angle graphene superlattices, Nature (London) **556**, 80 (2018).

[16] X. Liang, Z. A. H. Goodwin, V. Vitale, F. Corsetti, A. A. Mostofi, and J. Lischner, Effect of bilayer stacking on the atomic and electronic structure of twisted double bilayer graphene, Phys. Rev. B **102**, 155146 (2020).

[17] H. Fu, J. Zhang, Z. Ding, H. Li, and S. Meng, Stacking-dependent electronic structure of bilayer silicene, Appl. Phys. Lett. **104**, 131904 (2014).

[18] K. M. McCreary, M. Phillips, H.-J. Chuang, D. Wickramaratne, M. Rosenberger, C. S. Hellberg, and B. T. Jonker, Stacking-

dependent optical properties in bilayer WSe_2, Nanoscale **14**, 147 (2021).
[19] N. Sivadas, S. Okamoto, X. Xu, C. J. Fennie, and D. Xiao, Stacking-dependent magnetism in bilayer CrI_3, Nano Lett. **18**, 7658 (2018).
[20] P.-J. Guo, X.-Q. Lu, W. Ji, K. Liu, and Z.-Y. Lu, Quantum spin hall effect in monolayer and bilayer $TaIrTe_4$, Phys. Rev. B **102**, 041109(R) (2020).
[21] R. Peng, Y. Ma, H. Wang, B. Huang, and Y. Dai, Stacking-dependent topological phase in bilayer $m Bi_2Te_4 (m =$ Ge, Sn, Pb), Phys. Rev. B **101**, 115427 (2020).
[22] J. Zhou, Q. Wang, Q. Sun, X. S. Chen, Y. Kawazoe, and P. Jena, Ferromagnetism in semihydrogenated graphene sheet, Nano Lett. **9**, 3867 (2009).
[23] A.-Y. Lu, H. Zhu, J. Xiao, C.-P. Chuu, Y. Han, M.-H. Chiu, C.-C. Cheng, C.-W. Yang, K.-H. Wei, Y. Yang, Y. Wang, D. Sokaras, D. Nordlund, P. Yang, D. A. Muller, M.-Y. Chou, X. Zhang, and L.-J. Li, Janus monolayers of transition metal dichalcogenides, Nat. Nanotechnol. **12**, 744 (2017).
[24] J. Zhang, S. Jia, I. Kholmanov, L. Dong, D. Er, W. Chen, H. Guo, Z. Jin, V. B. Shenoy, L. Shi, and J. Lou, Janus monolayer transition-metal dichalcogenides, ACS Nano **11**, 8192 (2017).
[25] K. Zhang, Y. Guo, Q. Ji, A.-Y. Lu, C. Su, H. Wang, A. A. Puretzky, D. B. Geohegan, X. Qian, S. Fang, E. Kaxiras, J. Kong, and S. Huang, Enhancement of van der waals interlayer coupling through polar janus mosse, J. Am. Chem. Soc. **142**, 17499 (2020).
[26] S.-Q. Li, C. He, H. Liu, L. Zhao, X. Xu, M. Chen, L. Wang, J. Zhao, and J. Gao, Dramatically enhanced second harmonic generation in janus group-iii chalcogenide monolayers, Adv. Opt. Mater. **10**, 2200076 (2022).
[27] X. Tang and L. Kou, 2D janus transition metal dichalcogenides: Properties and applications, Physica Status Solidi (b) **259**, 2100562 (2022).
[28] D. Xiao, W. Yao, and Q. Niu, Valley-Contrasting Physics in Graphene: Magnetic Moment and Topological Transport, Phys. Rev. Lett. **99**, 236809 (2007).
[29] W. Yao, D. Xiao, and Q. Niu, Valley-dependent optoelectronics from inversion symmetry breaking, Phys. Rev. B **77**, 235406 (2008).
[30] S. M. Young and C. L. Kane, Dirac Semimetals in Two Dimensions, Phys. Rev. Lett. **115**, 126803 (2015).
[31] T. Zhou, J. Zhang, H. Jiang, I. Žutić, and Z. Yang, Giant spin-valley polarization and multiple hall effect in functionalized bismuth monolayers, npj Quantum Mater. **3**, 39 (2018).
[32] C. Niu, G. Bihlmayer, H. Zhang, D. Wortmann, S. Blügel, and Y. Mokrousov, Functionalized bismuth films: Giant gap quantum spin hall and valley-polarized quantum anomalous hall states, Phys. Rev. B **91**, 041303(R) (2015).
[33] K. He, Y. Wang, and Q.-K. Xue, Topological materials: Quantum anomalous hall system, Annu. Rev. Condens. Matter Phys. **9**, 329 (2018).
[34] C.-X. Liu, S.-C. Zhang, and X.-L. Qi, The quantum anomalous hall effect: Theory and experiment, Annu. Rev. Condens. Matter Phys. **7**, 301 (2016).
[35] J. Wang, B. Lian, and S.-C. Zhang, Quantum anomalous hall effect in magnetic topological insulators, Phys. Scr. **T164**, 014003 (2015).
[36] C.-Z. Chang and M. Li, Quantum anomalous hall effect in time-reversal-symmetry breaking topological insulators, J. Phys.: Condens. Matter **28**, 123002 (2016).
[37] C.-Z. Chang, J. Zhang, X. Feng, J. Shen, Z. Zhang, M. Guo, K. Li, Y. Ou, P. Wei, L.-L. Wang, Z.-Q. Ji, Y. Feng, S. Ji, X. Chen, J. Jia, X. Dai, Z. Fang, S.-C. Zhang, K. He, Y. Wang *et al.*, Experimental observation of the quantum anomalous hall effect in a magnetic topological insulator, Science **340**, 167 (2013).
[38] J.-X. Yin, W. Ma, T. A. Cochran, X. Xu, S. S. Zhang, H.-J. Tien, N. Shumiya, G. Cheng, K. Jiang, B. Lian, Z. Song, G. Chang, I. Belopolski, D. Multer, M. Litskevich, Z.-J. Cheng, X. P. Yang, B. Swidler, H. Zhou, H. Lin *et al.*, Quantum-limit chern topological magnetism in $TbMn_6Sn_6$, Nature (London) **583**, 533 (2020).
[39] Y. Deng, Y. Yu, M. Z. Shi, Z. Guo, Z. Xu, J. Wang, X. H. Chen, and Y. Zhang, Quantum anomalous hall effect in intrinsic magnetic topological insulator $MnBi_2Te_4$, Science **367**, 895 (2020).
[40] C. Liu, Y. Wang, H. Li, Y. Wu, Y. Li, J. Li, K. He, Y. Xu, J. Zhang, and Y. Wang, Robust axion insulator and chern insulator phases in a two-dimensional antiferromagnetic topological insulator, Nat. Mater. **19**, 522 (2020).
[41] H. Li, S.-Y. Gao, S.-F. Duan, Y.-F. Xu, K.-J. Zhu, S.-J. Tian, J.-C. Gao, W.-H. Fan, Z.-C. Rao, J.-R. Huang, J.-J. Li, D.-Y. Yan, Z.-T. Liu, W.-L. Liu, Y.-B. Huang, Y.-L. Li, Y. Liu, G.-B. Zhang, P. Zhang, T. Kondo *et al.*, Dirac Surface States in Intrinsic Magnetic Topological Insulators $EuSn_2As_2$ and $MnBi_{2n}Te_{3n+1}$, Phys. Rev. X **9**, 041039 (2019).
[42] G. Xu, B. Lian, and S.-C. Zhang, Intrinsic Quantum Anomalous Hall effect in the Kagome Lattice $Cs_2LiMn_3F_{12}$, Phys. Rev. Lett. **115**, 186802 (2015).
[43] J.-Y. You, C. Chen, Z. Zhang, X.-L. Sheng, S. A. Yang, and G. Su, Two-dimensional weyl half-semimetal and tunable quantum anomalous hall effect, Phys. Rev. B **100**, 064408 (2019).
[44] C. Niu, H. Wang, N. Mao, B. Huang, Y. Mokrousov, and Y. Dai, Antiferromagnetic Topological Insulator with Nonsymmorphic Protection in Two Dimensions, Phys. Rev. Lett. **124**, 066401 (2020).
[45] N. Sun, X. Wang, and W. Mi, Induced half-metallic characteristics and enhanced magnetic anisotropy in the two-dimensional janus $V_2I_3Br_3$ monolayer by graphyne adsorption, Phys. Chem. Chem. Phys. **23**, 17338 (2021).
[46] Z. Li, J. Zhang, and B. Zhou, Electric polarization related dirac half-metallicity in mn-trihalide janus monolayers, Phys. Chem. Chem. Phys. **22**, 26468 (2020).
[47] Z. Guan, N. Luo, S. Ni, and S. Hu, Tunable electronic and magnetic properties of monolayer and bilayer janus $Cr_2Cl_3I_3$: A first-principles study, Mater. Adv. **1**, 244 (2020).
[48] C. Zhang, Y. Nie, S. Sanvito, and A. Du, First-principles prediction of a room-temperature ferromagnetic janus vsse monolayer with piezoelectricity, ferroelasticity, and large valley polarization, Nano Lett. **19**, 1366 (2019).
[49] J. He and S. Li, Two-dimensional janus transition-metal dichalcogenides with intrinsic ferromagnetism and half-metallicity, Comput. Mater. Sci. **152**, 151 (2018).
[50] P. Giannozzi, S. Baroni, N. Bonini, M. Calandra, R. Car, C. Cavazzoni, D. Ceresoli, G. L. Chiarotti, M. Cococcioni, I. Dabo, A. D. Corso, S. de Gironcoli, S. Fabris, G. Fratesi, R. Gebauer, U. Gerstmann, C. Gougoussis, A. Kokalj, M. Lazzeri,

L. Martin-Samos *et al.*, QUANTUM ESPRESSO: A modular and open-source software project for quantum simulations of materials, J. Phys.: Condens. Matter **21**, 395502 (2009).

[51] P. Giannozzi Jr, O. Andreussi, T. Brumme, O. Bunau, M. B. Nardelli, M. Calandra, R. Car, C. Cavazzoni, D. Ceresoli, M. Cococcioni, N. Colonna, I. Carnimeo, A. D. Corso, S. de Gironcoli, P. Delugas, R. A. DiStasio, A. Ferretti, A. Floris, G. Fratesi, G. Fugallo *et al.*, Advanced capabilities for materials modelling with quantum ESPRESSO, J. Phys.: Condens. Matter **29**, 465901 (2017).

[52] J. P. Perdew, K. Burke, and M. Ernzerhof, Generalized Gradient Approximation Made Simple, Phys. Rev. Lett. **77**, 3865 (1996).

[53] D. Vanderbilt, Soft self-consistent pseudopotentials in a generalized eigenvalue formalism, Phys. Rev. B **41**, 7892(R) (1990).

[54] A. I. Liechtenstein, V. I. Anisimov, and J. Zaanen, Density-functional theory and strong interactions: Orbital ordering in mott-hubbard insulators, Phys. Rev. B **52**, R5467(R) (1995).

[55] M. Cococcioni and S. de Gironcoli, Linear response approach to the calculation of the effective interaction parameters in the LDA + U method, Phys. Rev. B **71**, 035105 (2005).

[56] N. Marzari, D. Vanderbilt, A. De Vita, and M. C. Payne, Thermal Contraction and Disordering of the Al(110) Surface, Phys. Rev. Lett. **82**, 3296 (1999).

[57] A. A. Mostofi, J. R. Yates, Y.-S. Lee, I. Souza, D. Vanderbilt, and N. Marzari, wannier90: A tool for obtaining maximally-localised wannier functions, Comput. Phys. Commun. **178**, 685 (2008).

[58] Q. Wu, S. Zhang, H.-F. Song, M. Troyer, and A. A. Soluyanov, Wanniertools: An open-source software package for novel topological materials, Comput. Phys. Commun. **224**, 405 (2018).

[59] Hongzhiwei Technology, Device Studio, Version 2021A, China (2021). See: https://iresearch.net.cn/cloudSoftware.

[60] R.-W. Zhang, Z. Zhang, C.-C. Liu, and Y. Yao, Nodal Line Spin-Gapless Semimetals and High-Quality Candidate Materials, Phys. Rev. Lett. **124**, 016402 (2020).

[61] X. Zhao, P.-j. Guo, F. Ma, and Z.-Y. Lu, Coexistence of topological weyl and nodal-ring states in ferromagnetic and ferrimagnetic double perovskites, Phys. Rev. B **103**, 085138 (2021).

[62] C. Niu, J.-P. Hanke, P. M. Buhl, H. Zhang, L. Plucinski, D. Wortmann, S. Blügel, G. Bihlmayer, and Y. Mokrousov, Mixed topological semimetals driven by orbital complexity in two-dimensional ferromagnets, Nat. Commun. **10**, 3179 (2019).

[63] H. Wang, N. Mao, C. Niu, S. Shen, M.-H. Whangbo, B. Huang, and Y. Dai, Ferromagnetic dual topological insulator in a two-dimensional honeycomb lattice, Mater. Horiz. **7**, 2431 (2020).

[64] M. Yamamoto, Y. Shimazaki, I. V. Borzenets, and S. Tarucha, Valley hall effect in two-dimensional hexagonal lattices, J. Phys. Soc. Jpn. **84**, 121006 (2015).

[65] X. Zhai and Y. M. Blanter, Spin-valley polarized quantum anomalous hall effect and a valley-controlled half-metal in bilayer graphene, Phys. Rev. B **101**, 155425 (2020).

[66] H. Pan, Z. Li, C.-C. Liu, G. Zhu, Z. Qiao, and Y. Yao, Valley-Polarized Quantum Anomalous Hall Effect in Silicene, Phys. Rev. Lett. **112**, 106802 (2014).